Electrical and Photoelectrochemical Characterization of CdS Particulate Films by Scanning Electrochemical Microscopy, Scanning Tunneling Microscopy, and Scanning Tunneling Spectroscopy

Xiao Kang Zhao,[1a] Larry McCormick,[1a] and Janos H. Fendler*,[1b]

Department of Chemistry, Syracuse University, Syracuse, New York 13244-4100, and J&D Scientific, Inc., 1815 West 1st Avenue, Mesa, Arizona 85202

Received April 10, 1991. Revised Manuscript Received July 2, 1991

Cadmium sulfide particulate films, generated at arachidic acid monolayer interfaces to 300 ± 50 Å thickness, have been in situ characterized by scanning tunneling microscopy (STM) under potentiostatic control. Electrical contact has been made between the tip of the scanning tunneling microscope, acting as the working electrode (WE) in contact with the CdS particulate film floating on aqueous 0.30 M NaCl, and the reference (RE) and counter (CE) electrodes, placed in the subphase. A well-defined single-reduction wave at about −1.15 V was observed. Prolonged exposure to room light shifted the reduction peak to −0.85 V. Electrical and photoelectrical characterizations have also been performed on Ti-foil-supported, 5000 Å thick CdS particulate films in an electrochemical cell. The Ti foil has been the WE, while the RE and CE have been placed into 0.50 M KCl, which bathed the CdS film. Cyclic voltammetry has been performed in the dark and under illumination in this system. Starting at about −0.9 V, the dark cathodic current had a peak at −1.15 V due to Cd^{2+} reduction and then the current rose to −1.4 V as a result of hydrogen production. The observed anodic peak at −0.85 V was attributed to the stripping of cadmium deposits in the lattice (Cd_L^0). Cyclic voltammetry subsequent to illumination resulted in the appearance of cathodic waves at −1.0 V and −1.3 V at the expense of that at −1.15 and in broadening of the anodic peak, indicating photocorrosion. Steady-state photocurrent measurements led to the estimation of the flat-band potential of the Ti-foil-supported CdS particulate film to be approximately −1.3 V. It also revealed the presence of weak intraband states at −1.0 V. STM images have also been taken of highly oriented pyrolytic graphite-supported, 300 ± 50 Å thick CdS particulate films, placed in a 0.50 M KCl solution as a function of electrochemical stripping and photocorrosion. Scanning tunneling spectroscopy of indium-coated, copper-substrate-supported, 100–200 Å thick CdS particulate films has been performed in air at fixed tip–sample distances. Rectification of n-type metal–insulator–semiconductor (MIS) junctions has been observed in the tunneling current vs. voltage curves. The determined diode ideality factor, n, of CdS particulate films was much larger than that found for bulk CdS (n = 1–2), indicating the termination of the depletion layer at the surface of size-quantized semiconductor particles in the film.

Introduction

Semiconductor particulate films have been generated in our laboratories at monolayer interfaces.[2-8] Controlled and slow infusion of hydrogen sulfide onto compressed monolayers prepared from cadmium and zinc arachidate resulted in the formation of covalent metal sulfide bonds at a large number of sites at the monolayer–aqueous interface.[3] Not more than a few molecules constituted the metal–sulfide nuclei at a given site. The initial nucleation resulted in the downward growth of well-separated, metal–sulfide microclusters that grew in height and width and coalesced into interconnected arrays of semiconductor particles. Further growth resulted in the formation of the "first layer" of a porous semiconductor film composed of 20–40 Å thick, 30–80 Å diameter particles. Adsorbed sulfide and/or bisulfite ions attracted metal cations in high local concentrations to the "first layer" of semiconductor particulate film, which in turn, seeded the formation of a new set of clusters and produced the "second layer" of porous particulate film. The process was then continued; the semiconductor particulate film grew layer by layer up to a plateau thickness (ca. 300 Å for CdS and ca. 3500 Å for ZnS) beyond which no semiconductor particle formation was observable. Similarly, cadmium selenide (CdSe) particulate semiconductor films were in situ generated at positively charged, dioctadecyldimethylammonium bromide (DODAB) monolayers floating on an aqueous subphase that contained appropriate concentrations of sodium selenosulfate and cadmium nitrilotriacetate.[7] Importantly, at any stages of their growth, the particulate films could be transferred to solid substrates without any structural reorganization.[4]

Absorption spectroscopy, X-ray diffraction, transmission electron microscopy, scanning tunneling microscopy, and electrical measurements of CdS and ZnS semiconductors, transferred to solid supports from monolayer interfaces, indicated the presence of mutually interacting quantum dots. Semiconductor size quantization is inherently interesting and often leads to altered mechanical, chemical, electrical, and electrooptical properties, which in turn may be exploited in a variety of applications.[9-13] Semiconductor particulate films, developed in our laboratories,[2-8] combine the advantages of nanoparticles, which provide a convenient route to size quantization, with that of bulk materials amenable to device fabrication. Size quantiza-

(1) (a) J&D Scientific. (b) Syracuse University.
(2) Zhao, X. K.; Yuan, Y.; Fendler, J. H. *J. Chem. Soc., Chem. Commun.* **1990**, 1248.
(3) Zhao, X. K.; Xu, S.; Fendler, J. H. *Langmuir* **1991**, *7*, 520.
(4) Zhao, X. K.; Fendler, J. H. *Chem. Mater.* **1991**, *3*, 168.
(5) Yuan, Y.; Cabasso, I.; Fendler, J. H. *Chem. Mater.* **1990**, *2*, 226.
(6) Yi, K. C.; Fendler, J. H. *Langmuir* **1990**, *6*, 1519.
(7) Zhao, X. K.; Fendler, J. H. *J. Phys. Chem.* **1991**, *95*, 3716.
(8) Zhao, X. K.; McCormick, L. D.; Fendler, J. H. *Langmuir* **1991**, *7*, 1255.
(9) Henglein, A. *Top. Curr. Chem.* **1988**, *143*, 113.
(10) Brus, L. A. *J. Phys. Chem.* **1986**, *90*, 2555.
(11) Steigerwald, M. L.; Brus, L. E. *Acc. Chem. Res.* **1990**, *23*, 183.
(12) Fendler, J. H. *Chem. Rev.* **1987**, *87*, 877.
(13) Andres, R. P.; Averback, R. S.; Brown, W. L.; Brus, L. E.; Goddard, W. A.; Kaldor, A.; Louie, S. G.; Moskovits, M.; Percy, P. S.; Riley, S. J.; Siegel, R. W.; Spaepen, F.; Wang, Y. *J. Mater. Res.* **1989**, *4*, 704.

0897-4756/91/2803-0922$02.50/0

tion has also been reported in chemically deposited cadmium selenide films[14] and, more recently, in cadmium sulfide coated porous polycrystalline titanium dioxide electrodes.[15]

Further characterization of size-quantized CdS particulate films is the subject of the present work. Four different approaches have been taken using scanning electrochemical microscopy (SECM),[16] scanning tunneling microscopy (STM),[16,17] and scanning tunneling spectroscopy (STS).[18-32] The first approach involved the in situ electrochemical characterization of 300 ± 50 Å thick CdS particulate films at the monolayer–aqueous solution interface. Electrical contact has been made between the tip of the STM, acting as the working electrode in contact with the CdS particulate film, and the reference and counter electrodes, placed in the subphase. In the second approach, the CdS particulate film was transferred to Ti foil, which acted as the working electrode. Reference and counter electrodes were placed in the solution that bathed the CdS particulate film. Dark and photocurrents have been determined as a function of voltage between the Ti foil and the substrate. In the third approach, STM images have been taken of highly oriented pryolytic graphite (HOPG) supported CdS particulate films, placed in a 0.50 M KCl solution, as a function of electrochemical stripping and photocorrosion. In the fourth approach, CdS particulate films have been examined in air on indium-coated copper substrates by STS.

Experimental Section

Arachidic acid (AA), cadmium sulfate, and sodium hydroxide (Sigma), sodium chloride, potassium chloride, spectroscopic grade chloroform, and ethanol (Fisher), high-purity dry N_2 (Union Carbide), and H_2S (Matheson) were used as received. Water (18 MΩ) was purified by using a Millipore Milli-Q system provided with a 0.22-μm Millistack filter at the outlet.

In situ generation of AA-monolayer-supported CdS semiconductor particulate films followed the described procedure.[3] AA-monolayer-supported CdS semiconductor particulate films were transferred to solid substrates by horizontal lifting through the surface layers. Highly oriented pyrolytic graphite (HOPG, ZYB grade, Union Carbide), indium-film-coated copper plates, and titanium foil (0.127 mm thick, 99.7% pure, Aldrich) were used as substrates for STM and STS.

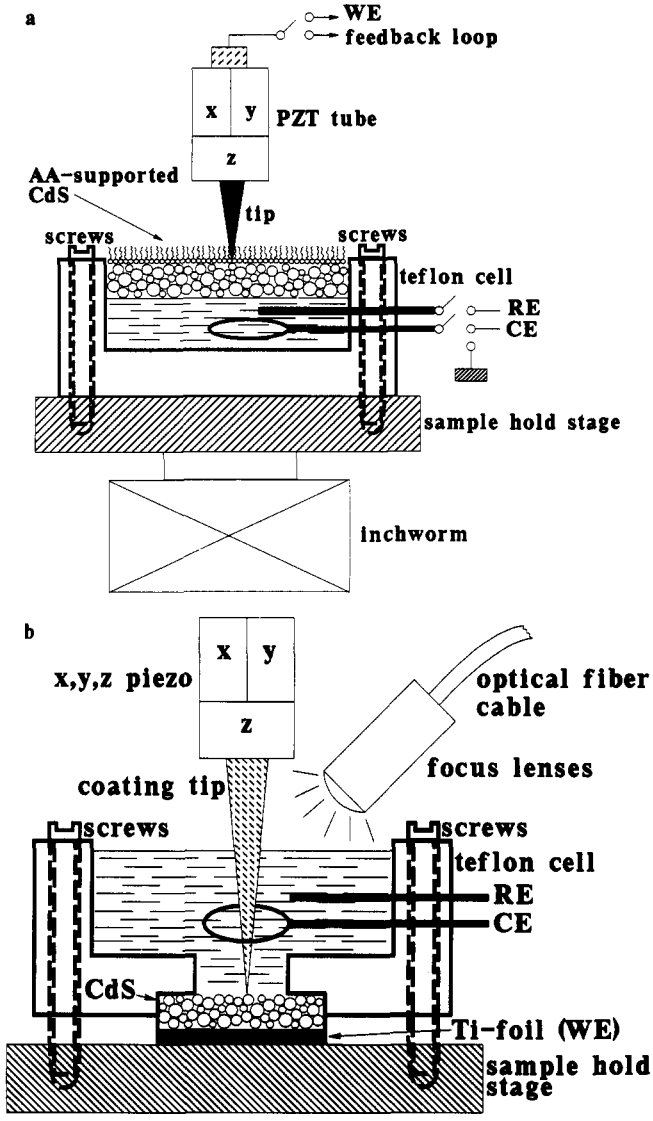

Figure 1. (a) Schematics of the cell used for electrochemical characterization of monolayer-supported CdS particulate films. WE = working electrode, RE = reference electrode, and CE = counter electrode. (b) Schematics of the photoelectrochemical cell used for characterization at Ti-foil-supported CdS particulate film. WE = working electrode, RE = reference electrode, and CE = counter electrode.

Using the STM tip as the working electrode (WE) in conventional potentiostatic experiments provided an oportunity to perform in situ electrochemical studies on CdS semiconductor particulate films formed at monolayer headgroup–aqueous subphase interfaces. The schematics of the electrochemical cell used for these experiments is illustrated in Figure 1a. Two methods were used for the preparation of AA-monolayer-supported, 300 ± 50 Å thick, CdS particulate films. In the first method, the films were in situ generated at aqueous cadmium ion solutions (1.0×10^{-3} M $CdSO_4$) in Teflon cells (15 mm in diameter, 5 mm high) equipped with Ag/AgCl wire reference electrodes (RE) and Pt ring counter electrodes (CE).[3] In the second method, a small Teflon cell was placed 2–5 mm under the surface in the well of a Lauda film balance (or a 7.0 cm^2 surface area, 4.0 cm deep, circular Pyrex trough) prior to film formation. Subsequent to the formation of the AA-monolayer-supported, 300 ± 50 Å thick CdS particulate film, the small Teflon electrochemical cell was gently lifted horizontally through the surface layers, transferred onto the sample hold stage of the STM, and tightly mounted with the four stage screws. After the screws were fastened, the Cd^{2+} subphase was completely replaced by a 0.3 M NaCl solution. The automatic "sample approach" system of the STM was used to

(14) Hodes, G.; Albu-Yaron, A.; Decker, F.; Motisuke, P. *Phys. Rev. B* **1987**, *36*, 4215.
(15) Vogel, R.; Pohl, K.; Weller, H. *Chem. Phys. Lett.* **1990**, *174*, 241.
(16) Bard, A. J.; Denualt, G.; Lee, G.; Mandler, D.; Wipf, D. O. *Acc. Chem. Res.* **1990**, *23*, 357.
(17) Binnig, G.; Rohrer, H. *Helv. Chim. Acta* **1982**, *55*, 726. Hansma, P.; Tersoff, J. *J. Appl. Phys.* **1987**, *61*, R1. Hansma, P. K.; Drake, B.; Marti, O.; Gould, S. N. C.; Prater, C. B. *Science* **1989**, *61*, 132.
(18) Kuk, Y.; Silverman, P. J. *Rev. Sci. Instrum.* **1989**, *60*, 165.
(19) Garcia, R.; Saenz, J. J.; Soler, J. M.; Garcia, N. *Surf. Sci.* **1987**, *181*, 69.
(20) Becker, R. S.; Golovchenko, J. A.; Hamann, D. R.; Swartzentruber, B. S. *Phys. Rev. Lett.* **1985**, *55*, 2032.
(21) Hamers, R. J.; Tromp, R. M.; Demuth, J. E. *Phys. Rev. Lett.* **1986**, *56*, 1972.
(22) Kaiser, W. J.; Jaklevic, R. C. *Surf. Sci.* **1987**, *181*, 55.
(23) Kaiser, W. J.; Bell, L. D.; Hecth, M. H.; Grunthaner, F. J. *J. Vac. Sci. Technol. A* **1988**, *6*, 519.
(24) Feenstra, R. M.; Stroscio, J. A. *J. Vac. Sci. Technol. B.* **1987**, *5*, 923.
(25) Stroscio, J. A.; Feenstra, R. M.; Newns, D. M.; Fein, A. P. *J. Vac. Sci. Technol. A* **1988**, *6*, 499.
(26) Feenstra, R. M.; Stroscio, J. A.; Tersoff, J.; Fein, A. P. *Phys. Rev. Lett.* **1987**, *58*, 1192.
(27) Feenstra, R. M.; Stroscio, J. A.; Fein, A. P. *Surf. Sci.* **1987**, *181*, 295.
(28) Jahannir, J.; West, P. E.; Young, A.; Rhodin, N. N. *J. Vac. Sci. Technol. A* **1989**, *7*, 2741.
(29) Fan, F.-R. F.; Bard, A. J. *J. Phys. Chem.* **1990**, *94*, 3761.
(30) Gilbert, S. C.; Kennedy, J. H. *Langmuir* **1989**, *5*, 1412.
(31) Kordic, S.; van Loenen, E. J.; Dijkkamp, D.; Hoeven, A. J.; Moraal, H. K. *J. Vac. Sci. Technol. A* **1989**, *8*, 549.
(32) Sakamati, K.; Hoh, A.; Gohshi, Y. *J. Vac. Sci. Technol. A* **1989**, *8*, 614.

bring the STM tip into contact with the AA-monolayer-supported CdS semiconductor particulate film. A relatively blunt, uninsulated Pt tip was rinsed in concentrated H_2SO_4 solution for 20–30 min, followed by rinsing by copious amounts of ultrapure water. The dried tip was placed in close proximity to the surface of the AA-monolayer-supported CdS particulate film and connected to the feedback loop circuit. The Pt ring was grounded to the sample hold stage (Figure 1a). The tip bias was set at +0.5 V with respect to the ground (i.e., Pt ring) during the "sample approach". The computer drove the continuous movement of the piezoelectric "inchworm", which brought the sample hold stage upward to the tip until it reached an acquired electrical current (by setting 1–2 nA in an "auto stop" mode). In this arrangement, a small ionic conduction current flows through the solution as a result of the contact between the tip and the AA-supported CdS particulate film. The electrochemical cell used for in situ measurements was set by switching the tip and Pt ring to the working electrode (WE) and counter electrode (CE), respectively, and connecting a Ag/AgCl wire to the reference electrode (RE) of the potentiostat. The entire system was covered by a plastic jar in order to diminish evaporation of water from the subphase. When needed, the system was purged by and kept under nitrogen.

Ti substrates (approximately 1 cm × 1 cm diameters and 0.127 mm thickness) were soaked in acetone, followed by etching in aqueous solutions of HF (4 wt %) and HNO_3 (30 wt %) for 30 s and copious rinsing in distilled water prior to further cleaning in distilled water in an ultrasonic cleaner for 20 min. AA-monolayer-supported, 300 ± 50 Å thick, CdS particulate films were transferred to Ti substrates by horizontal lifting through the surface layer of the trough. Subsequent to transferring to Ti foil, the films were dried in a N_2 atmosphere, and the AA monolayers were removed by gentle rinsing with ethanol (HPLC grade). The films were then heated at 300–400 °C for 15–20 min under nitrogen and subsequently cooled to room temperature for 0.5 h. The sequential transfers followed the same procedure until the CdS particulate films approached 5000 Å in thickness (16 successive transfers). These Ti-supported, CdS particulate films were rinsed with deionized water and etched for 3 s in 2 M HCl. Subsequent to rinsing in ultrapure water and drying under nitrogen, the samples were promptly used for the electrochemical experiments.

Photoelectrochemical measurements of solid-supported CdS particulate films were performed using a computer-controlled electrochemical potentiostat incorporated into a TAK 3.0 scanning tunneling microscope (Angstrom Technology, Mesa, AZ). Photoelectrochemical experiments on Ti-supported, CdS particulate films were carried out in a standard, one-compartment electrochemical cell that consisted of a 15 mm diameter Teflon cell (volume of 0.5 mL) with a 5 mm diameter well to accommodate the STM tip. The Teflon cell was sealed to the substrate with four screws at the sample hold stage. The Ti-foil substrate, supporting the CdS particulate film, acted as the working electrode (WE). Provision was made for the insertion of a Ag/AgCl wire reference electrode (RE) and a Pt ring counter electrode (CE), as shown in Figure 1b.

Both the cell and the electrode surfaces were carefully rinsed by acetone and copious amounts of distilled water prior to further cleaning in distilled water in an ultrasonic cleaner for 15–20 min. The pH of the electrolyte was adjusted by NaOH or HCl. Purified nitrogen was used to flush the electrolyte for 15 min for experiments where oxygen had to be precluded.

In photocurrent measurements, the potential control was established with the potentiostat. A 50 W fiber optic illuminator (LS S7/110, Fiberoptic Specialties, Inc.) was used to illuminate the sample (Figure 1b). Ag/AgCl and Pt ring electrodes were carefully shielded by black Teflon tubes to minimize the generation of light-induced electrode potentials and currents. Dark voltammograms of half cycles from $V + \Delta V$ to $V - \Delta V$ were stored by using the "background option" of the potentiostat. The small linear voltage ramp range, $2\Delta V$, was 20–40 mV. The appropriate photovoltammogram was then carried out at the current on-screen voltammogram. The photocurrent at the applied potential, V, was obtained by subtracting the dark voltammogram stored in the background option from the current on-screen photovoltammogram.

STM images in electrolyte solutions under potentiostatic conditions were obtained by using a TAK 2.0 STM, an instrument that was designed for electrochemistry. Subsequent to transferring the CdS particulate film to freshly cleaved HOPG and drying, the films were gently rinsed with ethanol and heated in N_2 at 300–400 °C for ca. 20 min. After cooling, HOPG-supported, 300 ± 50 Å thick CdS particulate films were placed in an electrochemical cell (Figure 1b). The STM tip was made by electrochemically etching a Pt–Ir wire (0.5 mm diameter). Faradaic current was reduced by coating the tip with Apiezon wax, leaving only the foremost 5 μm of the tip exposed. Tips were selected that had a tip/electrolyte interface capacitance of less than 10 pF and a leakage (i.e., ionic conduction current) of less than 100 pA with 1 V applied across a 1.0 M aqueous NaOH solution. The STM was operated in a constant current mode. Typical operating parameters were a tunneling current of 1 nA, tip bias voltage of 0.5–1.0 V, and scanning rate of 5 lines/s. Images were plotted on a CP 200U Mitsubishi color videocopy processor.

Using a scanning tunneling microscope (Nanoscope II, Digital Instruments, Inc.), the scanning tunneling spectra (current vs. voltage, I–V curves) were measured at fixed air gaps between the platinum tip and the CdS semiconductor particulate film surfaces. The 100–200 Å thick, CdS particulate films were transferred to indium-film-coated copper plates that served as ohmic contacts. If necessary, the AA monolayers were removed by gentle rinsing with ethanol. The I–V curves of STS were obtained by gating the feedback loop of the STM. Bringing the Pt tip to the desired height above the sample surface was accomplished by putting the feedback loop into action (i.e., to control the z-piezo) in a constant current mode of operation with a −0.9 V tip bias (with respect to the sample). The feedback loop was then opened, the distance between the tip and the sample was held stationary, the voltage between the tip and the sample was ramped, and the tunneling current was measured as a function of bias voltage. After the measurements were performed, the feedback loop was closed. The sampling period was taken as 100–150 μs.

Electrode potentials given in this paper are relative to the Ag/AgCl electode.

Results and Discussion

In Situ Electrochemistry of AA-Monolayer-Supported CdS Particulate Films. The 300 ± 50 Å thick, AA-monolayer-supported CdS particulate films were intact.[5] The nanosized tip and the computer-controlled approach with atomic level resolution of the STM allowed the in situ electrochemical measurements of monolayer-supported CdS particulate films in the cell shown in Figure 1a.

The dark current–potential curves (I–V) of a 300 Å thick CdS particulate film floating on 0.3 M NaCl are shown in Figure 2a. The scan was initiated at 0 V and first proceeded in the negative direction at a rate of 500 mV/s. Blank experiments in the absence of a CdS particulate film were performed on an AA-monolayer floating on a 0.3 M NaCl aqueous solution (see the insert in Figure 2a). A well-defined single reduction wave at about −1.15 V was observed in the initial scans (second to sixth cycles) after bringing the Pt tip into contact with the monolayer-supported, CdS particulate film (Figure 2a). The first scan was unstable because of a liquid capillary rise at the tip. This wave was attributed to O_2 reduction in acid solution:

$$O_2 + 4H_3O^+ + 4e^- \rightarrow 6H_2O \quad (1)$$

and in alkaline solution:

$$O_2 + 2H_2O + 4e^- \rightarrow 4OH^- \quad (2)$$

No reduction wave was observed in the absence of O_2. The same reduction wave was previously reported for the Cd surface (0001) at CdS electrodes.[33] This result is in good agreement with that observed for CdS particulate films having Cd-rich hexagonal lattice structures.[7] Pro-

(33) Meissner, D.; Memming, R.; Kastening, B. *J. Phys. Chem.* **1988**, *92*, 3476.

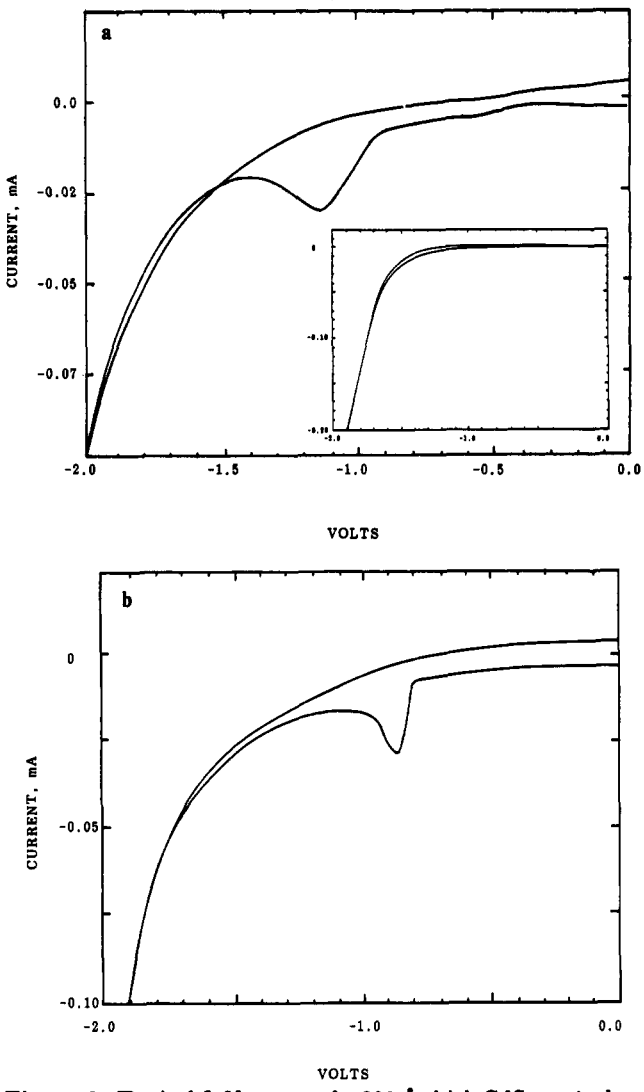

Figure 2. Typical *I–V* curves of a 300 Å thick CdS particulate film, floating on 0.30 M aqueous NaCl at pH = 6.8 in the dark (a) and subsequent to 6 h exposure to room light (b). The *I–V* curve of an AA monolayer (in the absence of CdS particles) under the same conditions is shown in the insert of Figure 2a. Scan rates were 500 mV/s using the cell illustrated in Figure 1a. Note differences in the scale.

longed exposure to room light (6 h) resulted in a positive shift to −0.85 V (Figure 2b). Oxygen reduction revealed that AA-monolayer-supported, CdS particulate films have much cleaner surfaces than those of solid-supported and even etched. The surface contamination of the latter may be due to surfactant removal and heating at high temperatures during successive film transfers.

Deposition of platinum (from the STM tip) to CdS can shift the potential for oxygen reduction and hydrogen production by about 0.45 V in the anodic direction. Absence of observable shifts confirmed that the platinum tip only acted as a metal contact and that most of the electrochemical reaction occurred at the CdS particulate film/electrolyte interface around the platinum tip.

Introducing HCl into the subphase (to give 6.7×10^{-2} M) of an AA-monolayer-supported CdS particulate film led to the appearance of an additional reduction wave and stripping peak, corresponding to reduction and oxidation reactions of Cd in the lattice. The blank experiment performed for AA monolayers (i.e., in the absence of CdS) appears in the insert in Figure 3.

Dark Voltammetry and Photocorrosion of Ti-Foil-Supported CdS Particulate Films in Contact with Aqueous Electrolytes. A typical dark voltammogram of a Ti-foil-supported, 5000 Å thick, CdS particulate film in contact with 0.5 M KCl is shown in Figure 4. The current–voltage (*I–V*) curve shows an n-type semiconductor–liquid junction behavior with dark rectifying characteristics; namely, there are very low dark currents at anodic potentials as high as +1.6 V and there are nearly exponential cathodic currents starting at about −1.4 V.

The effect of illumination on the current–voltage behavior of a Ti-foil-supported, 5000 Å thick CdS particulate film in an aqueous, air-saturated, 0.5 M KCl solution (pH = 6.8) is displayed in Figure 5. The dark cathodic current (scan i in Figure 5) started at about −0.9 V (Ag/AgCl) during the negative scan. A well-defined cathodic wave appeared at about −1.15 V, and then the current rose to about −1.4 V as a result of hydrogen production.[33-36] On the reverse positive scan, an anodic peak at about −0.85 V was observed. The cathodic peak at −1.15 V (scan i in Figure 5) is attributable to the irreversible electroreduction of Cd^{2+} ions in the CdS lattice:[34,37]

$$CdS + 2e^- \rightarrow Cd_L^0 + S^{2-}_{aq} \quad (3)$$

where the subscript L refers to the crystal lattice. Similarly, the anodic peak at −0.85 V is explicable in terms of the stripping of the Cd_L^0 deposit:

$$Cd_L^0 + 2h^+ \rightarrow Cd^{2+} \quad (4)$$

The reduction wave at ~−1.15 V and the corresponding stripping peak at −0.85 V were associated with electrochemical (EC) dissolution of CdS particulate films.

Cyclic voltammograms (curves ii), taken after 2 min of illumination at 0 (Figure 5a) and +1.5 V (Figure 5b), revealed new features. Well-defined cathodic waves at about −1.0 and −1.3 V replaced the wave at ~−1.15 V (see scan i). The height of the reduction wave at −1.0 V was quite sensitive to the time and intensity of illumination. The oxidation peak of Cd^0 broadened and shifted slightly to the anodic direction.

CdS has been extensively used in the conversion of solar energy into electrical or chemical energy.[38] The photoelectrochemical (PEC) conversion and stabilization of CdS electrodes have been of particular concern.[39-42] Photocorrosion of CdS in the presence of oxygen has recently been described in terms of[33,43]

$$CdS \xrightarrow{h\nu} e^- + h^+ \quad (5)$$

$$CdS + 4h^+ + H_2O + O_2 \rightarrow Cd^{2+}_{aq} + SO_4^{2-} + 4H^+ \quad (6)$$

$$O_2 + 4e^- + 2H^+ \rightarrow 2OH^- \quad (7)$$

The net stoichiometry indicates sulfate and cadmium ions to be the main photoproducts:[43]

$$CdS + 2O_2 \xrightarrow{h\nu} Cd^{2+}_{aq} + SO_4^{2-} \quad (8)$$

(34) Kolb, D. N.; Gerischer, H. *Electrochim. Acta* **1973**, *18*, 987.
(35) Masuda, H.; Fujishima, A.; Honda, K. *Chem. Lett.* **1980**, 1153.
(36) Meissner, D.; Memming, R.; Kastening, B.; Bahnemann, D. *Chem. Phys. Lett.* **1986**, *127*, 419.
(37) Ferrer, I. J.; Salvador, P.; Velasco, J. G. *J. Electronanal. Chem.* **1985**, *189*, 363.
(38) Grätzel, M. *Acc. Chem. Res.* **1981**, *14*, 376.
(39) Bard, A. J.; Wrighton, M. S. *J. Electrochem. Soc.* **1977**, *124*, 1706.
(40) Rajeshwar, K.; Kaneko, M.; Yamada, A.; Novfi, R. N. *J. Phys. Chem.* **1985**, *89*, 806.
(41) Natan, M. J.; Thakeray, J. M.; Wrighton, M. S. *J. Phys. Chem.* **1986**, *90*, 4089.
(42) Santangelo, P. G.; Miskelly, G. M.; Lewis, N. S. *J. Phys. Chem.* **1988**, *92*, 6359.
(43) Meissner, D.; Memming, R.; Li, S.; Jesodharam, S.; Grätzel, M. *Ber. Bunsen-Ges. Phys. Chem.* **1985**, *89*, 301.

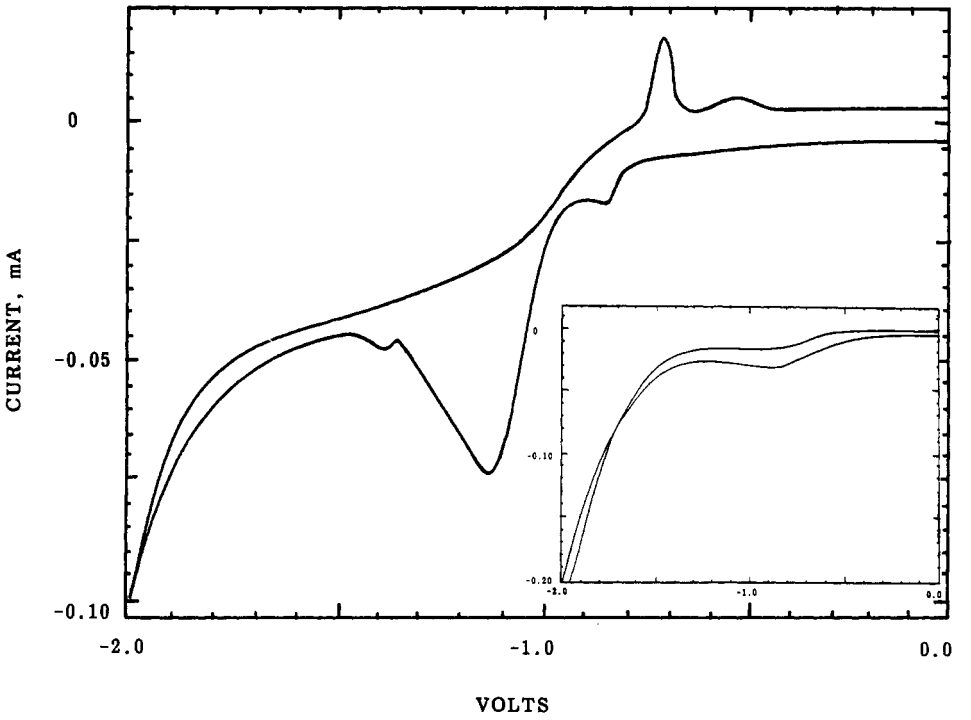

Figure 3. Typical $I-V$ curves of a 300 Å thick CdS particulate film, floating on 0.30 M aqueous NaCl in the dark. Subsequent to CdS particulate generation, HCl was added to the solution to give 6.7×10^{-2} M concentration. The $I-V$ curve of an AA monolayer (in the absence of CdS particles) on a solution of 0.30 M NaCl and 6.7×10^{-2} M HCl under the same conditions is shown in the insert. Scan rates were 500 mV/s using the cell illustrated in Figure 1a. Note the differences in the scale.

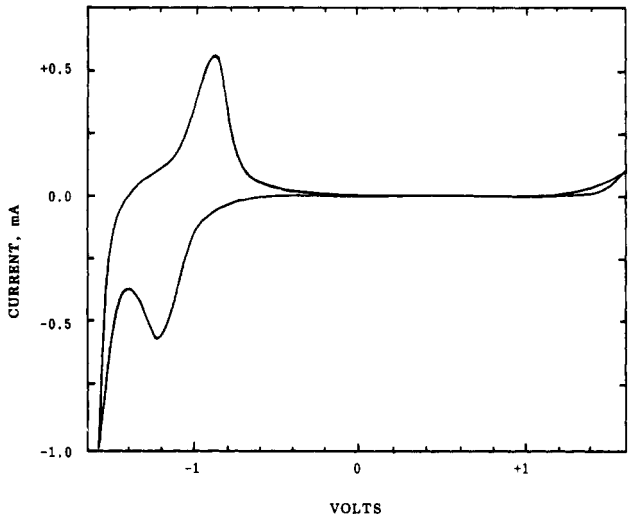

Figure 4. Typical current–voltage (tip vs. substrate), $I-V$, behavior of a Ti-foil-supported, 5000 Å thick CdS particulate film in air-saturated, aqueous 0.50 M KCl (pH = 6.8). The CdS particulate film was in situ generated at AA-monolayer/air saturated 0.30 M NaCl interfaces at pH = 6.8, transferred to a Ti-foil substrate by horizontal lifting, annealed at 300–400 °C and briefly (3 s) etched in 2.0 M HCl. Scan rates were 100 mV/s using the cell illustrated in Figure 1b.

The additional peak at −1.0 V (see scan ii in Figure 5) is attributable to the electrodeposition of cadmium ions onto the CdS particle surface:

$$Cd_s^{2+} + 2e^- \rightarrow Cd_s^0 \quad (9)$$

where the subscript s denotes surface-adsorbed soluble ions.

The height of the reduction wave at −1.0 V increased with increasing illumination times as a result of higher coverage at the surface and higher concentrations of Cd_s^{2+} in the nanosized pores of CdS semiconductor particulate films. The height decrease at the reduction wave with increases in the interval period between light off and the subsequent scan was interpreted in terms of lowering Cd^{2+} concentrations by diffusion out of the porous CdS particulate films. The negative shift to about −1.3 V for the cathodic wave (compare scan ii with scan i of Figure 5), originating in the electroreduction of Cd^{2+} ions from the lattice (eq 3), was probably due to a small potential drop across the photogenerated surface species of sulfur and sulfur/oxygen.[33]

Sulfur species deposited on the CdS surface during the photocorrosion reaction are attributed to the well-known reaction

$$CdS + 2H_2O \xrightarrow{h\nu} H_2 + Cd^{2+}_{aq} + S + 2OH^- \quad (10)$$

especially in cases where there was not enough oxygen at the PEC cell.[33,36,41,44]

The anodic peak, corresponding to the stripping of Cd_s^0 deposit from the surface, seems to shift slightly to the positive direction by comparison with that for the stripping of Cd_L^0 from the lattice via eq 4. This can be clearly observed in a dark voltammogram following 6 min of illumination at +1.5 V (Figure 5c). Prolonged illumination (10–15 min) at +1.5 V bias decreased the CdS film thickness, which was manifested in an irreversible change. Specifically, both the amplitude of the reduction wave and the height of the stripping peaks decreased.

Photocurrent and Flat-Band Potential Measurements of Ti-Foil-Supported CdS Particulate Films in Contact with Aqueous Electrolytes. The relative energies of semiconductor band edges at surfaces are usually estimated from the flat-band potential, V_{fb}, which can be determined by the measurement of potential-dependent capacitances (i.e., from the Mott–Schottky plot) or photocurrents.[45-48] Values of V_{fb} could not be estimated from

(44) Ellis, A. B.; Karas, B. R. *J. Am. Chem. Soc.* **1979**, *101*, 236.
(45) Ellis, A. B.; Kaiser, S. W.; Bolts, J. M.; Wrighton, M. S. *J. Am. Chem. Soc.* **1977**, *99*, 2839.

Mott–Schottky plots since they were, as expected, curvilinear.

Flat-band potentials could, however, be estimated from photocurrent potential plots. The steady-state photocurrent was measured directly for Ti-supported, 5000 Å thick, CdS film (0.2 cm^2) immersed in 0.5 M KCl (pH = 6.8, Figure 6). Neglecting recombination and thermal generation of carriers under radiation, the photogenerated hole current density through the reverse-biased depletion layer, j_P, is given by[49]

$$j_P = j_{PD} + j_{PB} = eI_0\left[1 - \frac{e^{-\alpha w}}{1 + \alpha L_P}\right] + eP_0\frac{D_P}{L_P} \quad (11)$$

where j_{PD} and j_{PB} are the minority carriers (i.e., the positively charged hole in a n-type semiconductor) generated in the depletion layer:

$$j_{PD} = -eI_0(e^{-\alpha w} - 1) \quad (12)$$

and at the depletion layer/bulk layer boundary:

$$j_{PB} = eI_0\frac{\alpha L_P}{1 + \alpha L_P}e^{-\alpha w} + eP_0\frac{D_P}{D_L} \quad (13)$$

where e is the electronic charge, I_0 is the effective light intensity, L_P is the hole diffusion length, D_P is the hole diffusion coefficient, α is the optical absorption coefficient, P_0 is the dark equilibrium hole concentration, and w is the depletion layer width and is given by

$$w = w_0(V - V_{fb})^{1/2} = \left[\frac{2\epsilon_s\epsilon_0(V - V_{fb})}{eN_{sc}}\right]^{1/2} \quad (14)$$

where w_0 is the depletion width at zero bias, V is the applied potential, ϵ_s is the relative dielectric constant of the semiconductor, ϵ_0 is the permittivity of the vacuum, and N_{sc} is the density of the charge in the space-charge region. At equilibrium, the hole concentration (P_0) is negligibly small. The second term can be neglected in comparison with the first term in eq 13. With $\alpha = 1 \times 10^4$ cm^{-1} at a wavelength of 500 nm for CdS particulate films,[4] L_P = (1–2) × 10^{-5} cm[48,50] and $\alpha L_P = 0.1$–$0.2 \ll 1$. The net hole current density for CdS particulate films is given by simplifying the expression

$$j_P = eI_0(1 - \exp[-\alpha w_0(V - V_{fb})^{1/2}]) \quad (15)$$

According to eq 15, the onset of photocurrent occurs at the flat-band potential (i.e., $V = V_{fb}$). The determined onset of the anodic photocurrent, and hence the flat-band potential, −1.3 V, agreed with values previously measured for CdS.[33,47,51]

In the photocurrent potential curve, a small sunken hole appeared at about −1.0 V. This value was approximately 0.3 V more positive than the flat-band potential. Similar behavior has been observed previously for CdS and CdSe semiconductors.[47,52–54] Holes in the I–V curves are attributed to intragap states that are capable of participating in electron transfer at the semiconductor–electrolyte boundary. There are several different forms of energy levels at the semiconductor surface, including intrinsic surface states, Lewis sites, and surface states arising from foreign species becoming adsorbed. These sites or surface

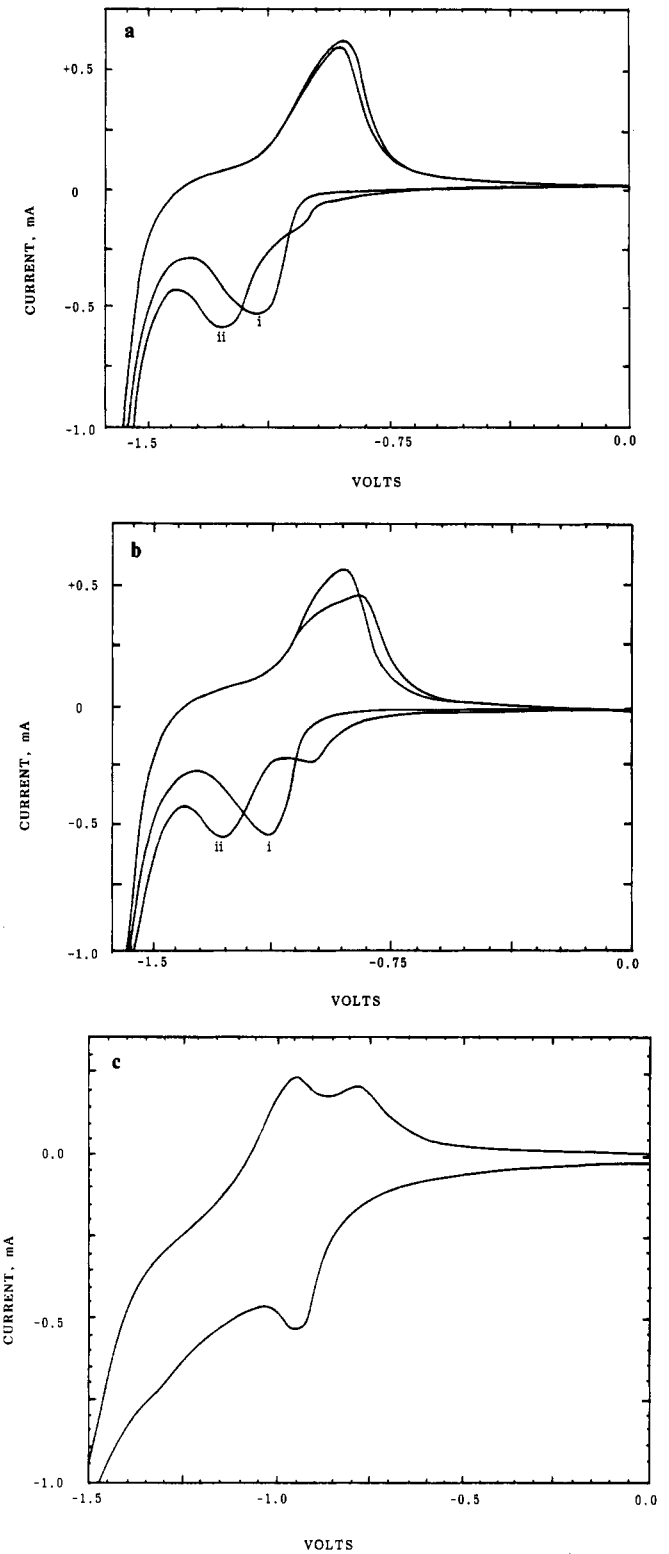

Figure 5. Typical current–voltage (tip vs. substrate), I–V, curves of a Ti-foil-supported, 5000 Å thick CdS particulate film in air-saturated, aqueous 0.50 M KCl (pH = 6.8) in the dark (i) and subsequent to 2 min of illumination (ii) at 0 (a) and +1.5 V (b) potential. The I–V curve in c was taken after 6 min of illumination at 1.5 V. The CdS particulate film was in situ generated at AA-monolayer interfaces at pH = 6.8, transferred to a Ti-foil substrate by horizontal lifting, annealed at 300–400 °C and briefly (3 s) etched in 2.0 M HCl. Scan rates were 100 mV/s using the cell illustrated in Figure 1b.

(46) Dimitrijevic, N. M.; Savic, D.; Micic, O.; Nozik, A. J. *J. Phys. Chem.* **1984**, *88*, 4278.
(47) Finlayson, M. F.; Wheeler, B. L.; Kakuta, N.; Park, K. H.; Bard, A. J.; Campion, A.; Fox, M. A.; Webber, S. E.; White, J. M. *J. Phys. Chem.* **1985**, *89*, 5676.
(48) Chmiel, G.; Gerischer, H. *J. Phys. Chem.* **1990**, *94*, 1612.
(49) Gärtner, W. W. *Phys. Rev.* **1954**, *116*, 84.
(50) Landolt-Börstein New Series; Springer: Berlin, 1982; Vol. 17a/b.
(51) Pentovelis, G.; Petit, J. P.; Chartier, P. In *Solar Energy Conversion and Storage*. Proceedings of the Sixth International Conference, 1986, D-23.
(52) Nagasubramanian, G.; Wheeler, B. L.; Hope, G. A.; Bard, A. J. *J. Electrochem. Soc.* **1983**, *130*, 385.
(53) Wheeler, B. L.; Hackerman, N. *J. Phys. Chem.* **1988**, *92*, 1601.
(54) Peter, L. M. *Chem. Rev.* **1990**, *90*, 753.

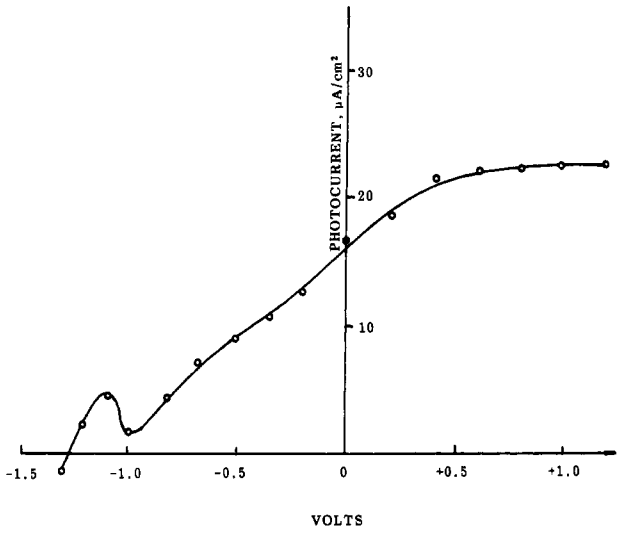

Figure 6. Steady-state photocurrent potential curve for a Ti-foil-supported, 5000 Å thick CdS particulate film (in situ generated at AA monolayer interfaces and transferred to the titanium-foil substrate, and subsequently annealed at 350 °C) in 0.50 M, air-saturated aqueous 0.50 M KCl (pH = 6.8) using the cell illustrated in Figure 1a.

states act as charge-carrier traps and lead to high surface recombination,[55] strong phototransients, and cathodic photoeffects that reduce the magnitude of the photoanodic current.

Energy levels associated with photooxidation products adsorbed at the CdS surface can be considered to be surface-state energy levels. Under illumination, the holes were photogenerated at semiconductor surfaces and became associated with the surface atoms as a result of surface lattice breakdown via eq 8 (in the presence of oxygen) or eq 10 (in the absence of oxygen). Photogenerated species, Cd_s^{2+} or S^0, tend to form acceptor surface states with bonding energies different from the intrinsic ionic surface state (i.e., Tamm state).[67] Indeed, the unoccupied energy levels associated with the surface species can be located below the energy of the conduction band in the gap region. Broadening of the adsorbate surface states into a surface heterogeneity makes the energy level of each adsorbate foreign species somewhat different from that of its neighbors.

The surface states, generated by photooxidation, strongly affect surface properties. Approximate mode and charge-transport mechanisms are schematically illustrated in Figure 7. The dark curent of CdS at negative potentials are transported via three processes: space-charge recombination, thermionic electron emission over the barrier, and quantum tunneling through the barrier (Figure 7a). Illumination leads to an additional process—inelastic tunneling through the surface state. Majority carrier transfer via surface states substantially increases the surface recombination velocity. To consider surface recombination, eq 15 is modified as

$$j_P = PeI_0(1 - \exp[-\alpha w_0(V - V_{fb})^{1/2}]) \quad (16)$$

where P is the charge-transfer probability given by[56,57]

$$P = u/(u + u_s) \quad (17)$$

u and u_s are charge-transfer velocities without surface states and surface recombination velocity, respectively.

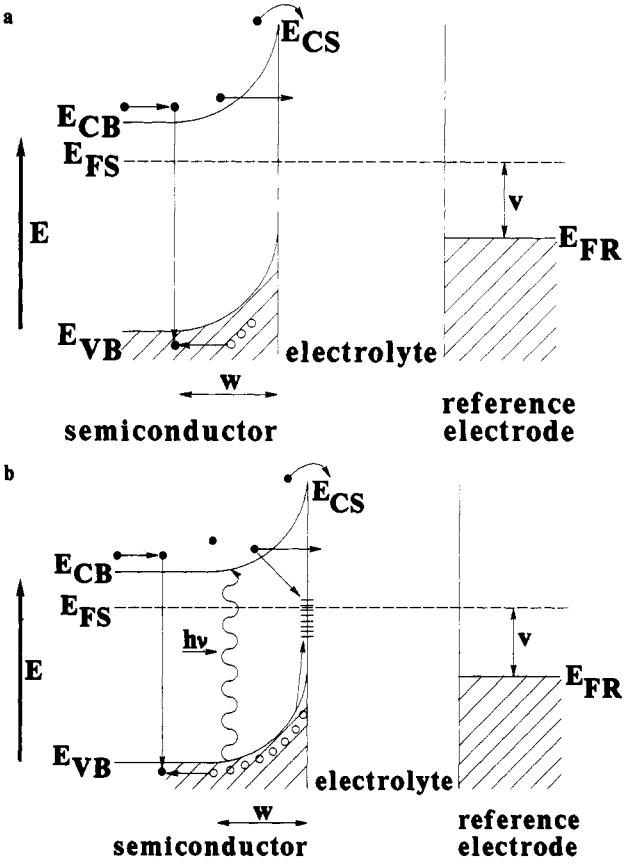

Figure 7. Charge-transport mechanisms at CdS particulate film–aqueous electrolyte junction in the dark (a) and under illumination (b). In the semiconductors, the highest occupied band state at equilibrium is the top of the valence band, E_{VB}; the lowest unoccupied state is the conduction band edge, E_{CB}; the two are separated in energy by the forbidden gap, E_{BG}, E_{FS} and E_{FR} are the Fermi levels of the semiconductor and the reference electrode, respectively, and V is the applied voltage.

Carrier recombination via surface states increases at the cathodic bias. Electron density at the surface is high, and surface recombination becomes favorable, which is manifested in decreased charge-transfer probability (i.e., $P < 1$).

Appearance of the sunken hole at −1.0 V potential may also be attributed to surface metal reduction, represented by eq 9. The photovoltammograms were similar, as shown in scan ii in Figure 5. Cd_s^0 metal clusters (differed from Cd_L^0) formed a new surface state, acting as charge traps, and modified the CdS semiconductor/electrolyte behavior.

Overall, photocurrent behavior suggests the presence of weak intragap states that cannot shift the flat-band potential of CdS particulate films in the anodic direction.

STM Images of HOPG-Supported CdS Particulate Films in Contact with Aqueous Electrolytes under Potential Control. Demonstration that the STM could be used to study samples immersed in aqueous solution has opened up the possibility for in situ electrode surface characterizations.[16,58-61] Potential- and photopotential-driven surface changes of CdS particulate films bathed in an electrolyte solution, were studied in the electrochemical cell shown in Figure 1b. Atomic flatness of HOPG renders it to be a very useful substrate for topographic investigations of CdS particulate films.

(55) Shockley, W.; Read, W. I. *Phys. Rev.* **1952**, *87*, 835.
(56) Pettingen, B.; Schöppel, H. R.; Gerischer, H. *Ber. Bunsen-Ges. Phys. Chem.* **1974**, *78*, 450.
(57) McCann, J. F.; Pezy, J. *J. Electrochem. Soc.* **1981**, *128*, 1735.
(58) Sonnenfeld, R.; Hansma, P. K. *Science* **1986**, *232*, 211.
(59) Itaya, K.; Sugawara, S. *Chem. Lett.* **1987**, 1927.
(60) Sonnenfeld, R.; Schardt, B. C. *Appl. Phys. Lett.* **1986**, *49*, 1172.
(61) Itaya, K.; Higaki, K.; Sugawara, S. *Chem. Lett.* **1988**, 421.

Immersing untreated, HOPG-supported, CdS particulate films (dried in a desiccator for several hours) into aqueous solutions resulted in a substantial loss of material. Annealing at 300–400 °C for 15–20 min in a nitrogen atmosphere increased the stability of HOPG-supported, 300 ± 50 Å thick CdS particulate films, but it also changed their optical and physical properties somewhat.

Absorption spectra of unannealed, quartz-supported, 300 ± 50 Å thick, CdS particulate films, in situ generated at AA monolayers, showed ca. 0.1 eV blue shifts of direct bandgap energy[4] with respect to the bulk semiconductor.[4,7,9-12] Recovery of the bulk bandgap energy of 2.4 eV upon heating suggested the collapse of the ultrafine CdS particulate film. Resistivities of unannealed, glass-supported, 300 ± 50 Å thick, CdS particulate films at room temperature were determined to be 10^7–10^8 Ω cm, which shows that the particulate films tend to act as an insulator.[4] Low conductivity of untreated, 300 ± 50 Å thick, CdS particulate films makes it more difficult to obtain good, clear STM images, even at high positive tip bias (≥1.5 V). Decreasing the resistivities to 1–10 Ω cm upon heating makes it possible to obtain STM images in the air or under solution.

A typical STM topography (220 nm × 220 nm) of an annealed, HOPG-supported, 300 ± 50 Å thick, CdS particulate film in 0.5 M KCl solution is shown in Figure 8a. For nonreactive surfaces, it has been shown that images obtained with the STM are virtually identical with the surface that is in contact with air.[18] STM images show that the annealed CdS particulate film consists of aggregated semiconductor particles. STM images observed for unannealed, HOPG-supported CdS particulate films revealed that interconnected, 30–40 Å thick, 30–80 Å diameter, disk-shaped CdS polyparticles constituted the "first layer" of the semiconductor particulate film (optical thickness of about 30–40 Å).[7] The grain size of annealed, HOPG-supported, 300 ± 50 Å thick, CdS particulate films is about 30–40 Å high and has a 100–300 Å diameter, which is relatively larger but still disk shaped. Relatively smooth surfaces and distinct grain boundaries can be observed in the STM images (Figure 8a).

Immediately after taking nonreactive images (Figure 8a), the system was prepared for electrochemical and photoelectrochemical processes by retracting the tip about 1 μm away from the semiconductor film surface, disconnecting it from the STM feedback circuit to prevent the electrochemical reaction from changing the structure of the film and then connecting it to the voltammograph. The semiconductor films were potentiostatically controlled with respect to the Ag/AgCl reference electrode. After the electrochemical treatment, the sample was held at the equilibrium potential (0 V), the tip was engaged again, and the surface was scanned at the previously scanned area.

Images taken after 3 and 10 cycles in the dark at scan rates of 100 mV/s between potentials of 0 and −1.6 V are shown in Figure 8b,c. The dark voltammogram showed a couple of well-defined cathodic waves at −1.2 V during the negative sweep and an anodic peak at about −0.9 V on the reverse scan for a HOPG-supported, 300 ± 50 Å, CdS film in 0.3 M NaCl. This cyclic voltammogram was somewhat similar to that observed for the Ti-foil-supported, 5000 Å CdS particulate film (Figure 4).

After 3 and 10 cycles, the coulometer recorded the total charge transfer of approximately 3 and 10 mC/cm^2 at the stripping of the Cd_L^0 deposit, which, assuming electrochemical corrosion, corresponds to the removal of 60 and 200 Å CdS particulate films, respectively. After 3 cycles, the grain size was reduced in comparison with nonreactive ones, and surface contamination was obviously observed. Surface contaminants can increase the noise level seen in the STM image (Figure 8b). After 10 dark cycles, large isolated CdS islands with very rough surfaces were detected on the atomically flat graphite surface. Furthermore, large areas of graphite surfaces became observable as the result of electrochemical stripping of the CdS particles from the HOPG substrate. Bonding between CdS particulate films and the carbon atoms of HOPG is apparently rather weak.

Surface topography of a CdS particulate film after illumination under the potentiostatic control was also found to be changed by photocorrosion. Surface features of 300 ± 50 Å thick, CdS particulate films in 0.5 M KCl (pH = 6.8) in the presence of O_2 after 5 and 15 min of illumination under white light at 0 V of sample potential are shown in Figure 9a,b, respectively. Coating of the CdS surfaces by the photodecompositions products made it difficult to distinguish features of individual particles (Figure 9a). More uniform corrosion led to surface migration and reconstruction (Figure 9a,b) instead of island formation by pure nonuniform electrochemical corrosion (Figure 8c). Anodic polarization at +1.2 V accelerated the photodecomposition procedure (Figure 9c) and prolonged photooxidation (15 mm at +1.2 V) led to the removal of almost all of the semiconductor films from the HOPG surface (Figure 9d).

Photocorrosion of CdS particulate films can also be determined by optical measurements. Absorption spectra revealed that illuminating a quartz-supported, 313 Å thick, CdS particulate film 15 and 20 min in a 0.5 M KCl aqueous solution decreased the optical thickness to 175 and 103 Å, respectively.

Surface Electronic Behavior of CdS Particulate Films in Air—Scanning Tunneling Spectroscopy. Scanning tunneling spectroscopy (STS) has been shown to be a powerful method for nanometer-scale resolution of electronic structures, energy bandgaps, flat-band potentials, and densities of surface states (DOS) at semiconductor surfaces.[18,27,29,62-67] In the present work, preimary interest has been focused on solid-state electronic characterization and size quantization effects on the Schottky tunneling junction behavior of CdS semiconductor particulate film, in situ formed at AA-monolayer interfaces.

I–V curves of indium-film-supported, 100–200 Å thick CdS films, obtained with the sample-and-hold technique for different tunneling currents at the tip bias of −0.9 V, are shown in Figure 10. A typical n-type rectification behavior is seen. At a given tip-to-sample separation, the current at forward bias behaved exponentially, while little current flowed under a reverse bias. At a large air gap (curve D in Figure 10), almost no current flowed in the reverse direction to 1.4 V. As the tip-to-sample distance decreased in the order of separation, D → C → B → A, the forward current increased. As the tip was brought closer to the surface, the electric field increased as a result of increased band bending.

The STM tip–semiconductor junction can be related to the metal–insulator–semiconductor (MIS) tunneling junction.[67] On the basis of the planar theory of Card and

(62) Avouris, P. *J. Phys. Chem.* **1990**, *94*, 2246.
(63) Itaya, K.; Tomita, E. *Surf. Sci.* **1989**, *219*, 2515.
(64) Chen, C. J. *J. Vac. Sci. Technol.* **1988**, *64*, 319.
(65) Lang, N. D. *Phys. Rev. Lett.* **1986**, *56*, 1164.
(66) Sakami, K.; Itoh, A.; Fujushima, A.; Gohshi, Y. *J. Vac. Sci. Technol.* **1990**, *A8*, 614.
(67) Sze, S. M. *Physics of Semiconductor Devices*; John Wiley: New York, 1981.

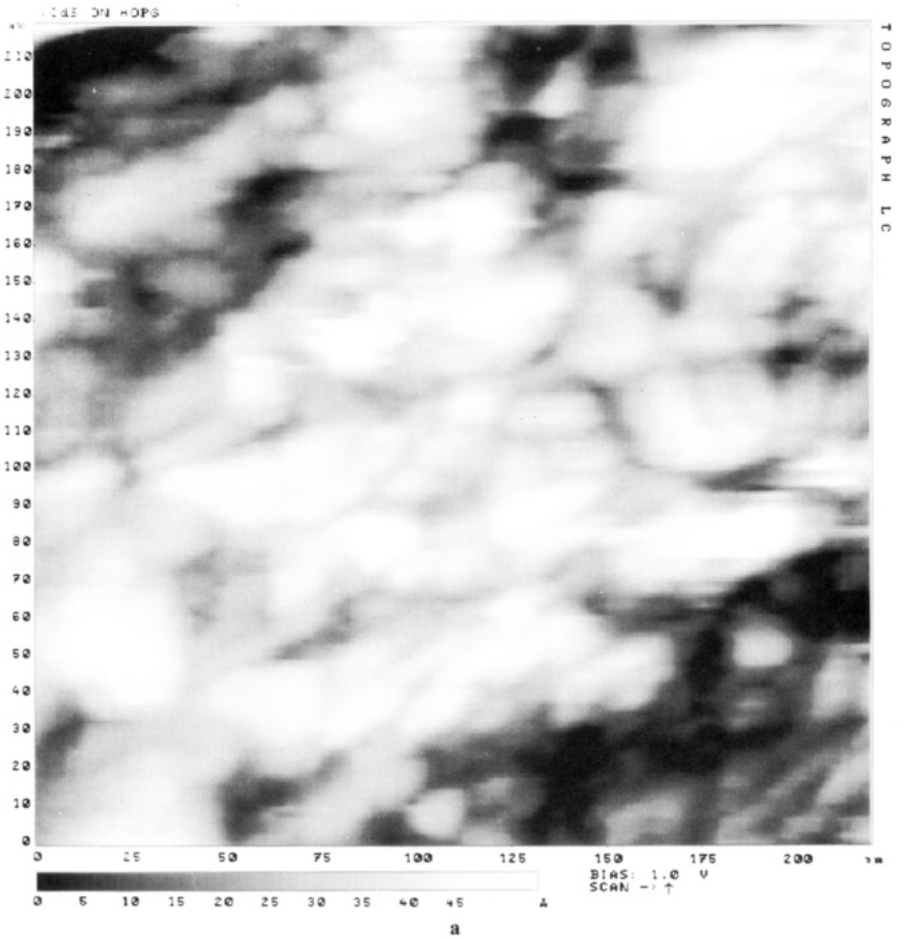

a

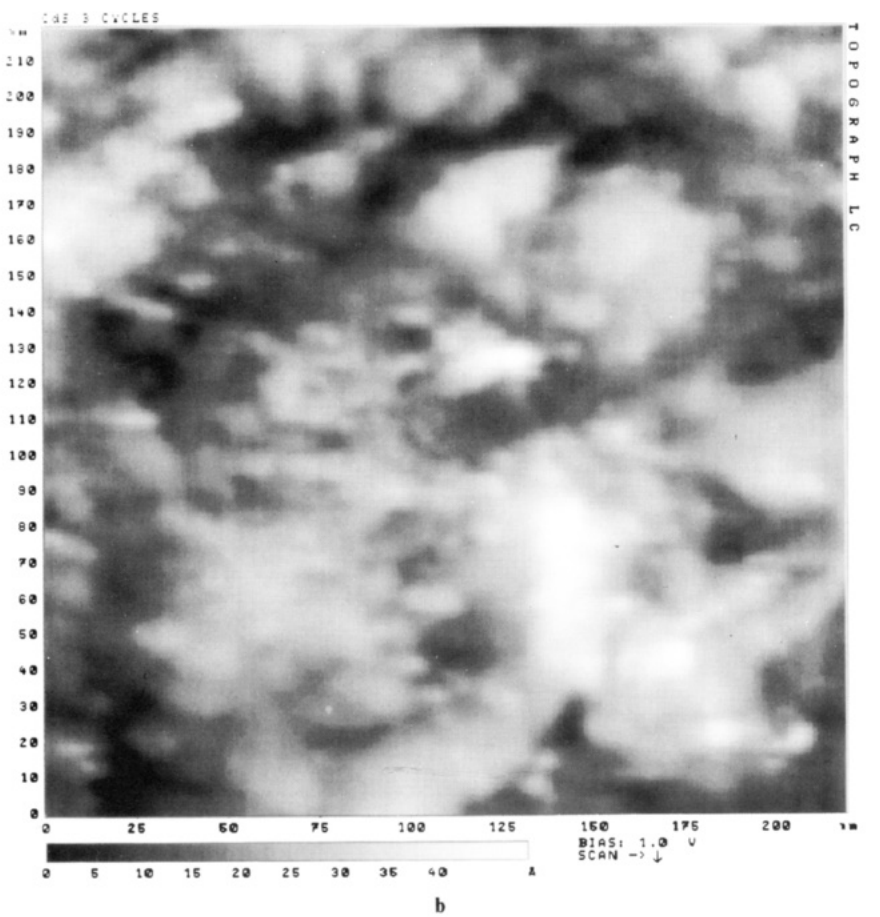

b

Figure 8. See caption on following page.

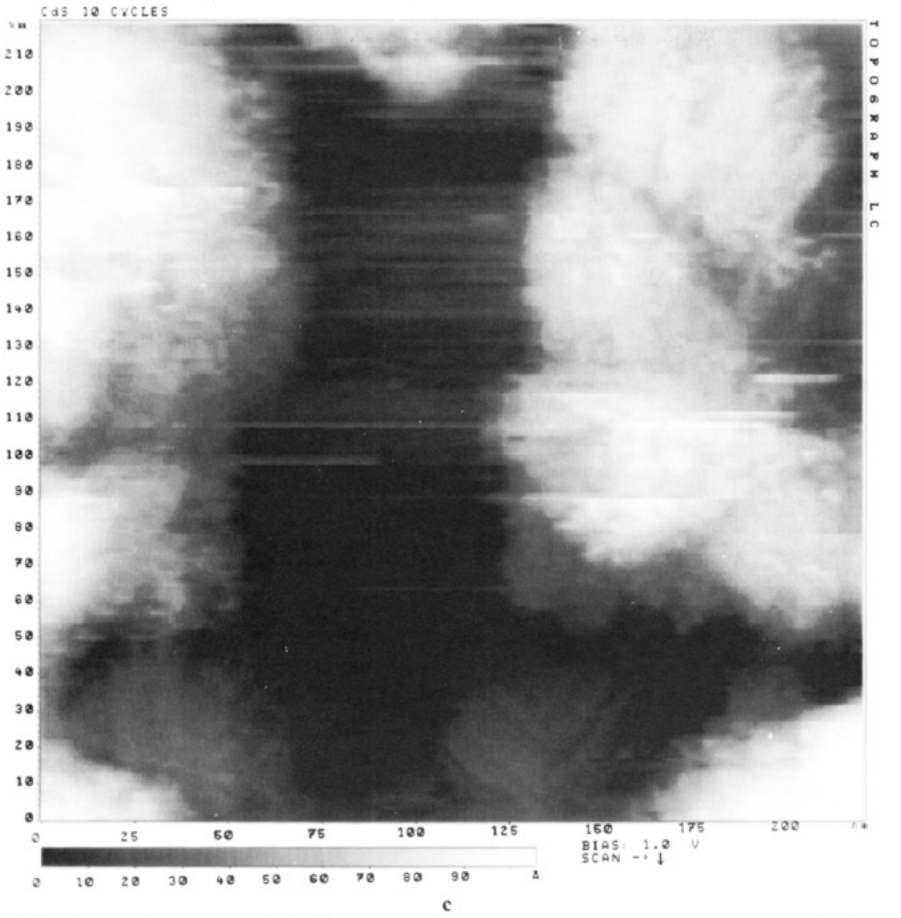

c

Figure 8. (a) Typical STM image of annealed, HOPG-supported, 300 ± 50 Å thick, CdS particulate film (nonreacted) in 0.5 M KCl solution. The tip bias was +1.0 V in the constant-current operation mode. The particulate films were prepared by the infusion of H_2S to cadmium arachidate monolayers. (b) Image of a HOPG-supported, 300 ± 50 Å thick, CdS particulate film in contact with 0.5 M KCl (pH = 6.8) in the presence of O_2 taken after three dark cycles at scan 100 mV/s between potentials of 0 and −1.6 V. (c) Image of a HOPG-supported, 300 ± 50 Å thick, CdS particulate film in contact with 0.5 M KCl (pH = 6.8) and the presence of oxygen, taken after 10 dark cycles at a scan rate of 100 mV/s between potentials of 0 V and −1.6 V.

Rhoderick, in the absence of surface state, the expression of tunneling current at forward bias is[68,69]

$$I = \frac{4\pi e}{\hbar}\sum_{K_t}\int_0^\infty |M_{sm}|^2\psi_s\psi_m(f_s - f_m)\,dE \qquad (18)$$

where $|M_{sm}|^2$ is the matrix element for the transition from the semiconductor to the metal, ψ_s and ψ_m are the density of state factors for the semiconductor and metal, f_s and f_m are the Fermi functions for the semiconductor and metal, K_t is the crystal momentum component transverse to the barrier, and E is the contribution to the energy due to the component of momentum perpendicular to the barrier. With the WKB approximation for the transmission coefficient of a rectangular barrier, the current density on forward bias due to the semiconductor conduction band electron tunneling into the metal leads to[69,70]

$$J = AT^2 \exp\left(-\frac{4\pi}{h}(2m\phi)^{1/2}s\right)\exp\left(\frac{-eV_{BO}}{kT}\right)\times \left[\exp\left(\frac{eV}{kT_n}\right) - 1\right] \qquad (19)$$

where s is the thickness of the insulator (i.e., the air gap here; see Figure 11), ϕ is the mean barrier presented by the insulator, V_{BO} is the barrier height at zero bias (see Figure 11), m is the electron mass, and Richardson's constant is $A = 4k^2\pi me/h^3$. The diode ideality factor, n, is given by

$$n = 1 + \frac{Skt_n}{\epsilon_i}\left(\frac{\epsilon_s}{w} + eD_s\right) \qquad (20)$$

where ϵ_i is the dielectric constant of the insulator and w is the depletion width, the same as that given by eq 14. In comparison with the relationship

$$J = J_s\left[\exp\left(\frac{eV}{nkT}\right) - 1\right] \qquad (21)$$

and saturation current density, $J_s = AT^2\exp(-eV_{BO}/kT)$, for metal–semiconductor Schottky diodes, eq 19 is modified by a tunneling exponent, $\exp(-(4\pi/h)(2m\phi)^{1/2}S)$. In the presence of an insulator, the majority carrier overcoming the potential barrier would have to tunnel through a distance S, the separation of metal and semiconductor as a result of the transmission coefficient decrease.

Employing the approximation for a rectangular barrier into the tip–semiconductor tunneling junction and assuming the constant densities of states for the tip, we can write the tunneling current density by multiplying a constant G for eq 19.[64,71-74]

$$J = AT^2G\exp\left(-\frac{4\pi}{h}(2m\phi)^{1/2}S\right)\exp\left(\frac{-eV_{BO}}{kT}\right)\times \left[\exp\left(\frac{eV}{nTk}\right) - 1\right] \qquad (22)$$

(68) Harrison, W. A. *Phys. Rev.* **1961**, *123*, 85.
(69) Card, H. C.; Rhoderick, E. H. *J. Phys. D* **1971**, *4*, 1589.
(70) Pande, K. P. *Phys. Status Solidi* **1977**, *42A*, 615.

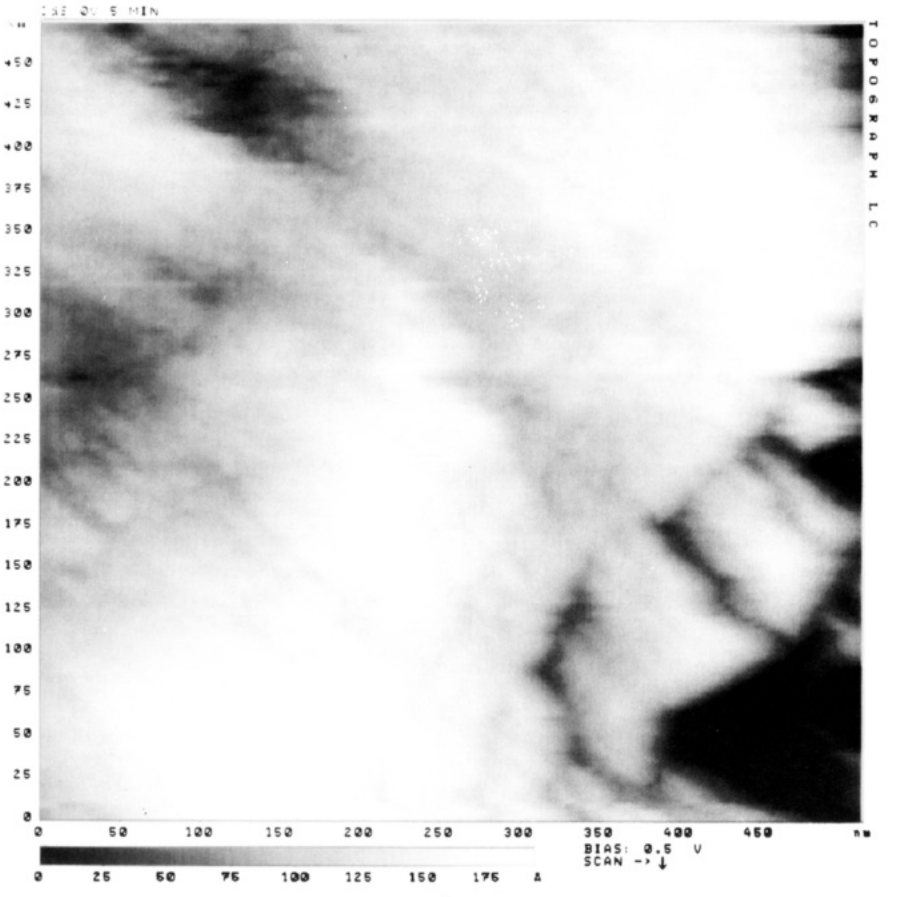

a

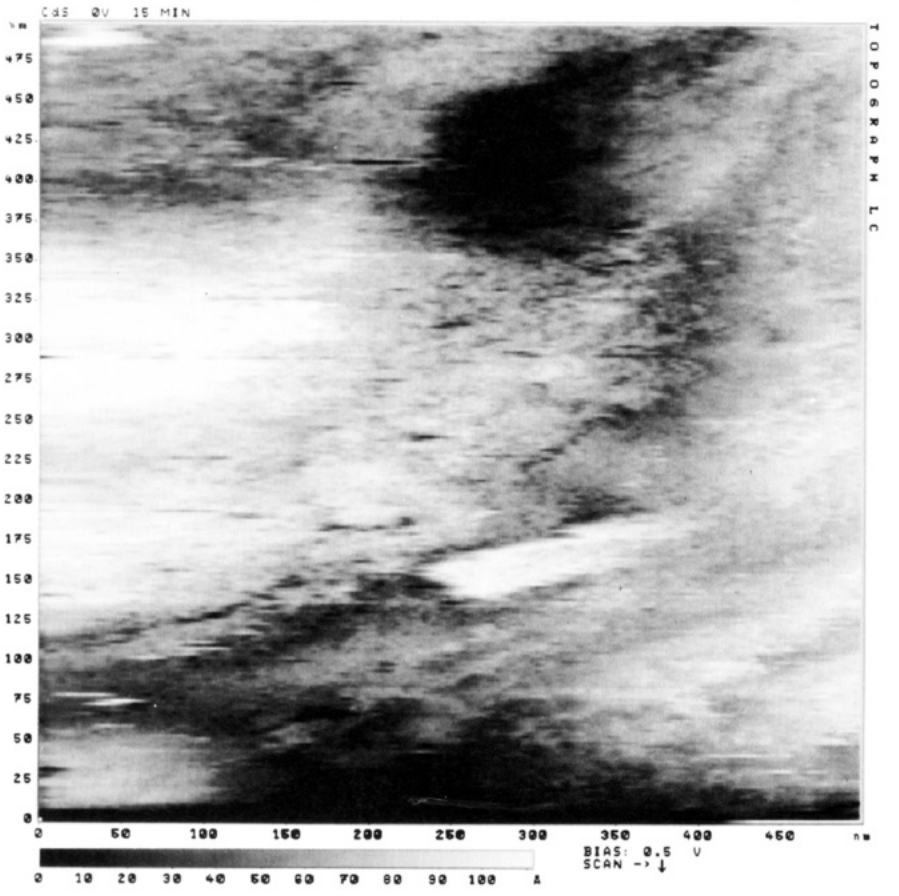

b

Figure 9. STM images of HOPG-supported, 300 ± 50 Å thick, CdS particulate films in 0.5 M KCl (pH = 6.8) in the presence of oxygen. The images were taken after photooxidation for 5 min at 0 V potential (a), 15 min at 0 V potential (b), 5 min at +1.2 V potential (c), and 15 min at +1.2 V potential (d).

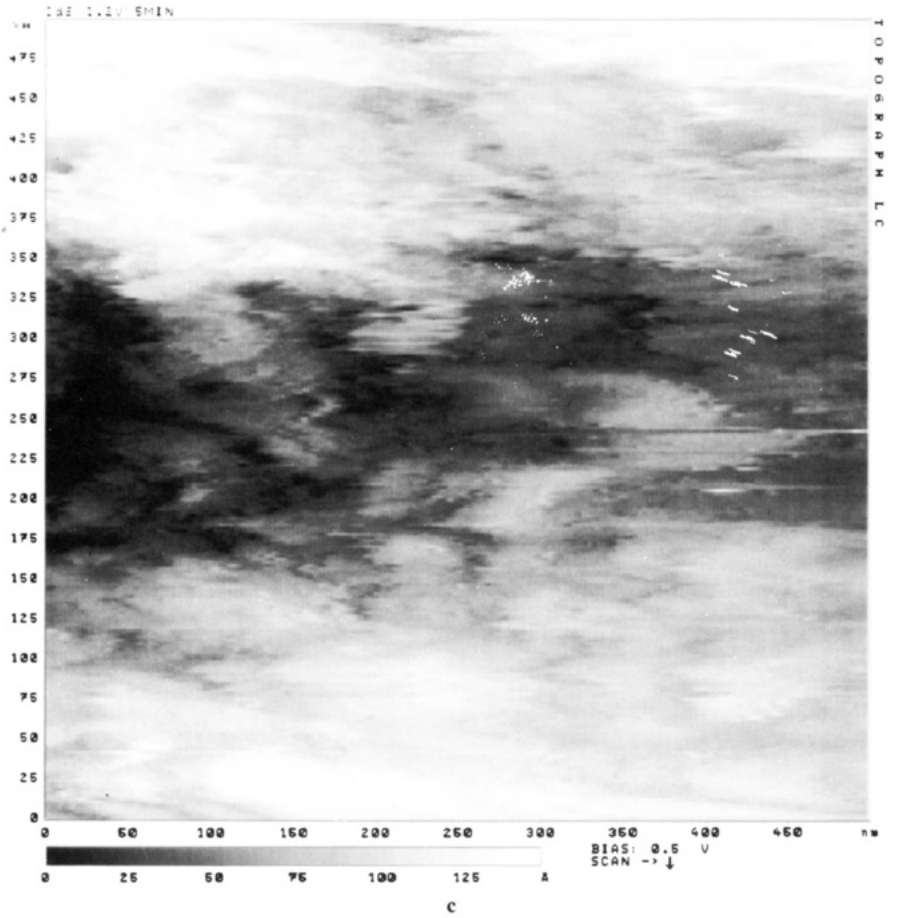

c

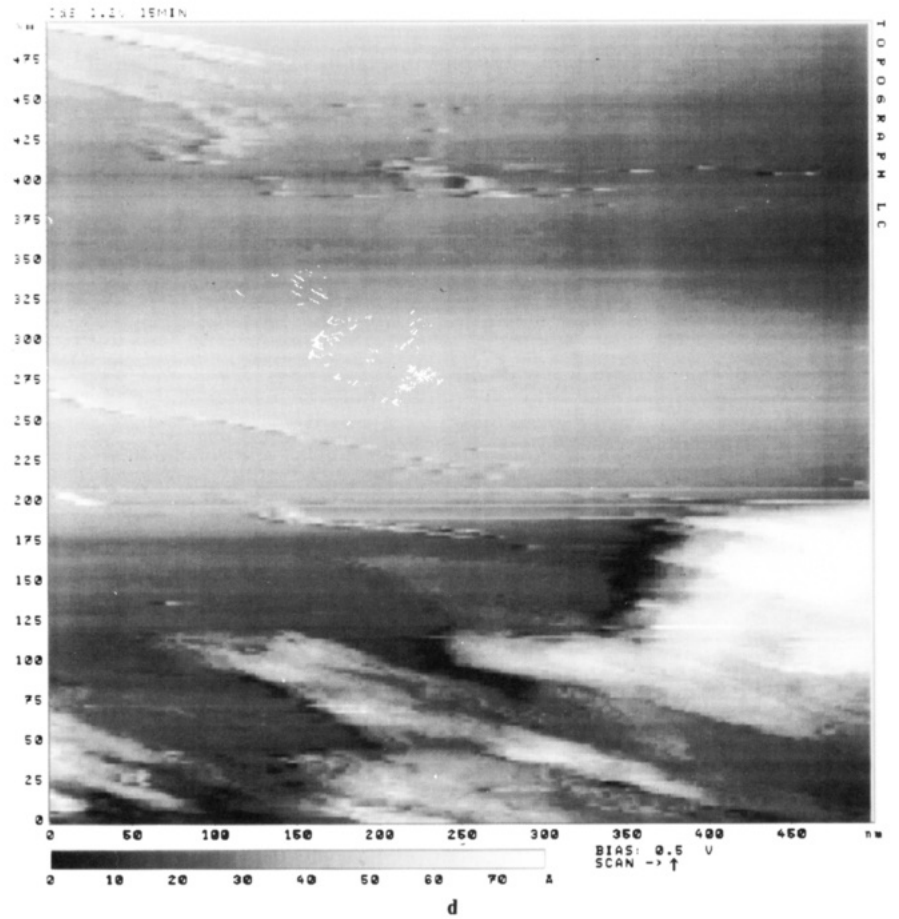

d

Figure 9. Continued.

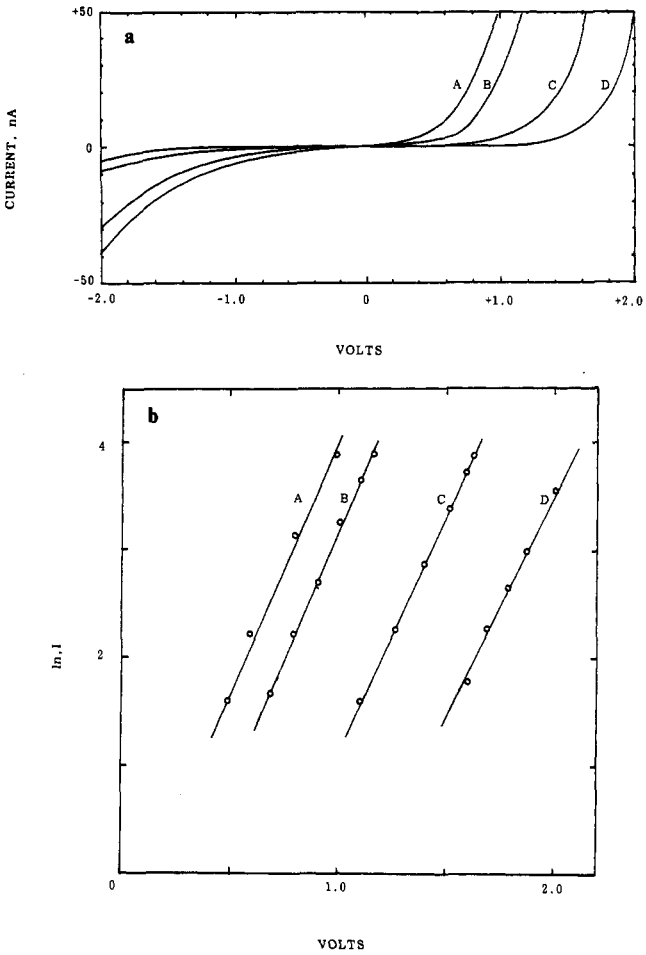

Figure 10. (a) Scanning tunneling spectroscopy of an indium-supported, 100–200 Å thick CdS particulate film, in situ generated at AA monolayer interfaces. I–V curves (tip vs. sample) at different tip–surface distances are plotted. The tip-to-sample distances increased in the order of A → B → C → D. (b) In I vs. V for the indium-film-supported, CdS particulate film. Semilogarithms were taken for curves A–D from Figure 11a.

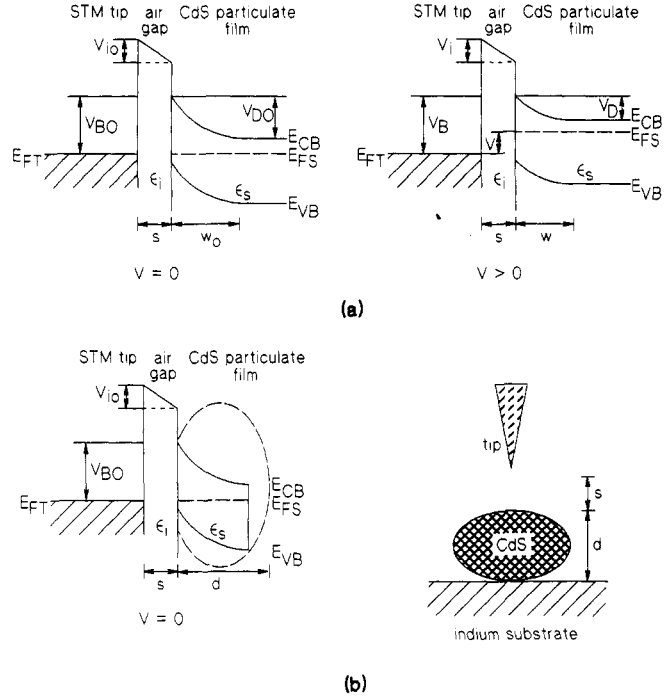

Figure 11. (a) Energy band diagram of MIS Schottky barrier at zero (left) and forward bias V (right). (b) The termination of the depletion layer width, w, at small particle surface, s and d are tip–sample distance and the thickness of disk-shaped particles, respectively. V_{DO}, V_{BO}, and V_{io} are surface potentials across the depletion layer, the barrier height, and the insulation layer at 0 bias; similarly, w_0 is the depletion width at zero bias. V_D, V_B, and V_i are surface potentials across the depletion layer, the barrier height, and the insulation layer at a forward bias, V, respectively. E_{VB}, E_{CB}, E_{FS}, and E_{FT} are the energies of the valence band, conduction band, Fermi level of the semiconductor, and Fermi level of the STM tip, respectively. ϵ_i = gap permittivity and ϵ_s = semiconductor permittivity.

where G is a constant depending on the geometry of the tip and sample.

For forward biases, $V > 3kT/e$, the second term in the square brackets of eq 22 (i.e., reverse current contribution due to metal electron tunneling into the semiconductor) can be neglected. So, for bias voltages in excess of $3\,kT/e$, the current–voltage semilogarithmic plot would show a linear behavior with the slope given by e/nkT.

The semilogarithmic I–V characteristics are clearly seen in Figure 10b. The diode ideality factor, n, at room temperature (23 °C), determined from the slopes, has been found to be 8.2, 8.4, 8.9, and 9.6 for curves A–D, respectively. For an ideal metal–semiconductor (MS) Schottky diode, $n = 1$. If the recombination currents were very small, slight increases of the n value (n = 1–2) for MIS tunneling diodes were attributed to altering of the surface potential in the semiconductor (i.e., V_{DO} at zero bias and V_D at forwared biases in Figure 11a) by the potential drop across the insulator.[69] The significant change of n values (n = 7.9–8.8) in the present work can be considered to be due to the size effects of CdS particulate films in situ formed on monolayer interfaces. STS tunneling junctions in the present work revealed the electronic properties of CdS particulate films to be different from those of bulk semiconductors.

Using $\epsilon_s = 5.7$[75] and $N_{sc} = 1.6 \times 10^{17}$ cm^{-3} [76] for n-type, monolayer-supported, CdS particles and taking $V - V_{fb} = 1$ V in eq 14 led to the depletion layer width $w = w_0 = 620$ Å. This value was much larger than the particle size, d, of CdS particulate films. Limiting the space charge region to the size of the semiconductor particles, d, terminates the depletion layer width at the surface,[14,77] i.e., $w \approx d$.

At low density of interface states and with neglect of the second term in brackets in eq 20, the particle size of CdS particulate films can be approximately determined by

$$d = w = \frac{S\epsilon_s}{\epsilon_i(n-1)} \qquad (23)$$

Applying $\epsilon_s/\epsilon_i = 5.7$ for CdS, $n \approx 9$ and tip–sample separation $S \approx 10$–30 Å[27,29] in eq 23 led to the particle's size $d \approx 15$–40 Å, which is in good agreement with the thickness of disk-shaped particles determined by STM.

STS tunneling junction behavior in the present work revealed that the electronic properties of CdS particulate films were different from those of bulk semiconductors as a result of the depletion layer termination at the particle surface (Figure 11b), which lowered surface potentials V_{DO}

(71) Tersoff, J.; Hamann, D. R. *Phys. Rev. Lett.* **1983**, *50*, 1998.
(72) Garcia, N.; Ocal, C.; Flores, F. *Phys. Rev. Lett.* **1980**, *50*, 2002.
(73) Feuchtwang, T. E.; Cutler, P. H.; Miskovsky, N. M. *Phys. Lett.* **1983**, *28*, 167.
(74) Tersoff, J.; Hamann, D. R. *Phys. Rev. B* **1985**, *31*, 805.
(75) Brus, L. E. *J. Phys. Chem.* **1983**, *79*, 5566.
(76) Zhao, X. K.; Baral, J.; Fendler, J. H. *J. Phys. Chem.* **1990**, *94*, 2043.
(77) Hodes, G.; Albu-Yaron, A. *Proc. Electrochem. Soc.*; Pennington, NJ, 1988.

and V_D and tended toward an insulator behavior.

Acknowledgment. Support of this research by grants from the Department of Energy (to J.H.F.) and the United States Army Research Office (to L.D.M.; Contract Number DAAL-03-90-C-0003) is gratefully acknowledged.

Registry No. CdS, 1306-23-6; Ti, 7440-32-6; H_2S, 7783-06-4; NaCl, 7647-14-5; In, 7440-74-6; KCl, 7447-40-7; O_2, 7782-44-7; H_2, 1333-74-0; arachidic acid, 506-30-9; graphite, 7782-42-5; cadmium arachidate, 14923-81-0.

Synthesis and Structure of a New Family of Cuprate Superconductors: $LnSr_2Cu_2GaO_7$

J. T. Vaughey,[†,§] J. P. Thiel,[‡,§] E. F. Hasty,[†] D. A. Groenke,[†,§] Charlotte L. Stern,[§] K. R. Poeppelmeier,*[,†,‡,§] B. Dabrowski,[†,⊥,∥] D. G. Hinks,[⊥] and A. W. Mitchell[⊥]

The Science and Technology Center for Superconductivity, Materials Research Center, and the Department of Chemistry, Northwestern University, Evanston, Illinois 60208; Materials Science Division, Argonne National Laboratory, Argonne, Illinois 60439; and Department of Physics, Northern Illinois University, DeKalb, Illinois 60115

Received April 10, 1991. Revised Manuscript Received July 16, 1991

The synthesis of layered cuprates with nonmagnetic and fixed oxidation state cations separating the Cu–O planes has, until now, led to nonsuperconducting materials. A new series of layered copper oxides with the general formula $LnSr_2Cu_2GaO_7$ (Ln = La–Yb, Y) has been synthesized. The structure has been studied by both powder neutron diffraction and single-crystal X-ray analysis. The typical unit cell is $a \approx 22.8$ Å, $b \approx 5.5$ Å, $c \approx 5.4$ Å, in space group *Ima*2 (No. 46). The structure is closely related to that of $YBa_2Cu_3O_7$ and can be described as replacement of the square-planar copper with a tetrahedral gallium. The larger lanthanides are distributed unevenly over the two A-cation sites, whereas the smaller lanthanides occupy the site between the cuprate planes. We have been able to introduce superconductivity in the Y–Sr–Cu–Ga–O system by appropriate doping with calcium and annealing.

Introduction

The importance of copper–oxygen layers in the high-temperature ($T_c > 35$ K) superconductors was realized in 1986[1] after the report by Bednorz and Müller on their work in the La–Ba–Cu–O system.[2] The conducting planes ($CuO_{4/2}$) of these materials result from the hybridization of the Cu(3d) and O(2p) orbitals, which form closely and symmetrically coordinated copper and oxygen atoms in square nets.[3] Other families of superconductors are $La_{2-x}M_xCuO_4$[1] (M = Ca^{2+}, Sr^{2+}, Ba^{2+}), $Nd_{2-x}Ce_xCuO_4$,[4] $YBa_2Cu_3O_{7-\delta}$,[5] $(Tl,Bi)_m(Ba,Sr)_2Ca_{n-1}Cu_nO_{m+2n+2}$[6,7] ($m$, n = integers), $Pb_2Sr_2LnCu_3O_{8+\delta}$[8] (Ln = lanthanides), and $La_{2-x}Sr_xCaCu_2O_6$.[9] All of these compounds can be described as an intergrowth of AO rocksalt layers with ABO_{3-x} perovskite units and have the general formula $(AO)_m(ABO_{3-x})_n$, where m and n are integers and B is copper. Although no theory on the mechanism of high-temperature superconductivity has gained acceptance, the observation of high-temperature superconductivity in this class of layered materials has led to a phenomenological understanding that superconductivity depends on the two-dimensional conducting planes with weak interplane coupling.

The influence of substitutions on superconductivity has been studied in great detail in $YBa_2Cu_3O_{7-\delta}$. All lanthanides have been substituted into the eight-coordinate yttrium position.[10] With the exception of praseodymium,[11] superconductivity is preserved. In contrast, the addition of small amounts of a transition or post-transition metal onto either the square-planar or square-pyramidal copper site generally resulted in the loss of superconductivity.[12]

† The Science and Technology Center for Superconductivity.
‡ Materials Research Center.
§ Department of Chemistry, Northwestern University.
⊥ Argonne National Laboratory.
∥ Northern Illinois University.
* To whom correspondence should be addressed.

(1) (a) Uchida, S.; Takagi, H.; Kitazawa, K.; Tanaka, S. *Jpn. J. of Appl. Phys.* **1987**, *26*, L1. (b) Takagi, H.; Uchida, S.; Kitazawa, K.; Tanaka, S. *Jpn. J. of Appl. Phys.* **1987**, *26*, L123. (c) Cava, R. J.; van Dover, R. B.; Batlogg, B.; Rietman, E. A. *Phys. Rev. Lett.* **1987**, *58*, 408.
(2) Bednorz, J. G.; Müller, K. A. *Z. Phys. B: Condens. Matter* **1986**, *64*, 189.
(3) (a) Yu, J.; Freeman, A. J.; Xu, J.-H. *Phys. Rev. Lett.* **1987**, *58*, 1035. (b) Mattheiss, L. F. *Phys. Rev. Lett.* **1987**, *58*, 1028.
(4) Tokuza, Y.; Takagi, H.; Uchida, S. *Nature* **1989**, *337*, 345.
(5) (a) Wu, M. K.; Ashburn, J. R.; Torng, C. J.; Hur, P. H.; Meng, R. L.; Gao, L.; Huang, Z.; Wang, Y. Q.; Chu, C. W. *Phys. Rev. Lett.* **1987**, *58*, 908. (b) Beno, M. A.; Soderholm, L.; Capone, D. W.; Jorgensen, J. D; Schuller, I. K.; Segre, C. U.; Zhang, K.; Grace, J. D. *Appl. Phys. Lett.* **1987**, *51*, 57. (c) You, H.; McMullan, R. K.; Axe, J. D.; Cox, D. E.; Liu, J. Z.; Crabtree, G. W.; Lam, D. J. *Solid State Commun.* **1987**, *64*, 739. (d) Siegrist, T.; Sunshine, S.; Murphy, D. W.; Cava, R. J.; Zahurak, S. M. *Phys. Rev. B* **1987**, *35*, 7137. (e) Simon, A.; Köhler, J.; Borrmann, H.; Gegenheimer, B.; Kremer, R. *J. Solid State Chem.* **1988**, *77*, 200.
(6) (a) Sheng, Z. Z.; Hermann, A. M. *Nature* **1988**, *332*, 55. (b) Subramanian, M. A.; Torardi, C. C.; Calabrese, J. C.; Gopalakrishnan, J.; Morrissey, J. J.; Askew, T. R.; Flippen, R. B.; Chowdhry, U.; Sleight, A. W. *Nature* **1988**, *332*, 420.
(7) (a) Michel, C.; Hervieu, M.; Borel, M. M.; Grandin, A.; Deslandes, F.; Provost, J.; Raveau, B. *Z. Phys. B* **1987**, *68*, 421. (b) Maeda, H.; Tanaka, Y.; Fukutomi, M.; Asano, T. *Jpn. J. Appl. Phys.* **1988**, *27*, L209. (c) Chu, C. W.; Bechtold, J.; Gao, L.; Hor, P. H.; Huang, Z. J.; Meng, R. L.; Sun, Y. Y.; Wang, Y. Q.; Xue, Y. Y. *Phys. Rev. Lett.* **1988**, *60*, 941. (d) Hazen, R. M.; Prewitt, C. T.; Angel, R. J.; Ross, N. L.; Finger, L. W.; Hadidiacos, C. G.; Veblen, D. R.; Heaney, P. J.; Hor, P. H.; Meng, R. L.; Sun, Y. Y.; Wang, Y. Q.; Xue, Y. Y.; Huang, Z. J.; Gao, L.; Bechtold, J.; Chu, C. W. *Phys. Rev. Lett.* **1988**, *60*, 1174.
(8) Cava, R. J.; Batlogg, B.; Karjewski, J. J.; Rupp, L. W.; Schneemeyer, L. F.; Siegrist, T.; van Dover, R. B.; Marsh, P.; Peck, W. F., Jr.; Gallagher, P. K.; Glarum, S. H.; Marshall, J. H.; Farrow, R. C.; Waszczak, J. V.; Hull, R.; Trevor, P. *Nature* **1988**, *336*, 211.
(9) Cava, R. J.; Batlogg, B.; van Dover, R. B.; Krajewski, J. J.; Waszczak, J. V.; Fleming, R. M.; Peck, W. F.; Rupp, L. W.; Marsh, P.; James, A. C. W. P.; Schneemeyer, L. F. *Nature* **1990**, *345*, 602.
(10) Hulliger, F.; Ott, H. R. *Z. Phys. B: Condens. Matter* **1987**, *67*, 291.
(11) Soderholm, L.; Goodman, G. L. *J. Solid State Chem.* **1989**, *81*, 121.

0897-4756/91/2803-0935$02.50/0